The static polarisability of metal clusters and spheres in an improved Thomas-Fermi approximation

1989 J. Phys.: Condens. Matter 1 10391

(http://iopscience.iop.org/0953-8984/1/51/012)

J. Phys.: Condens. Matter **1** (1989) 10391–10405. Printed in the UK

The static polarisability of metal clusters and spheres in an improved Thomas–Fermi approximation

Ll Serra†, F Garcias†, M Barranco†, J Navarro‡, L C Balbás§, A Rubio§ and A Mañanes‖

† Departament de Física, Universitat de ses Illes Balears, E-07071 Palma de Mallorca, Spain

‡ Departament de Física Atòmica, Molecular i Nuclear and Instituto de Física Corpuscular, CSIC-Universitat de València, E-46100 Burjassot, València, Spain

§ Departamento de Física Teórica, Atómica y Nuclear, Universidad de Valladolid, E-47011 Valladolid, Spain

‖ Departamento de Física Moderna, Universidad de Cantabria, E-39005 Santander, Spain

Received 2 May 1989

Abstract. We have used an approximate Thomas–Fermi–Dirac–Weizsäcker functional to evaluate the static polarisability of clusters and spheres of metallic atoms for excitation operators of the kind $r^L Y_{L0}$. Calculations for Na and Ag systems made of up to $N = 1000$ atoms have been carried out in the spherical jellium approximation for multipolarities $L =$ 1 to 15. These results have been combined with others obtained previously by the authors to estimate the width of the surface resonance and its evolution with L.

1. Introduction

Each electronic property exhibited by small metallic clusters as a function of their size converges towards the bulk surface value in a different manner that is not always well understood [1]. Among these properties, the surface response to an applied multipolar field, in particular the static electric polarisability of metal microparticles, is an important electronic property related to the screening of the external field from the interior of the microparticle. Due to the high surface-to-volume ratio in these systems, quantum size effects must be taken into account carefully if one wants to have a realistic description of the electron response.

Early calculations of the polarisability of small metallic spheres [2–5] predicted values of the dipolar polarisability α smaller than the classical value $\alpha_{Cl} = R^3$, where R is the radius of the sphere. However, more recent calculations [6–15] lead to polarisabilities enhanced with respect to α_{Cl}. This enhancement is essentially due to the induced electronic density outside the boundary of the positive charge (electronic spill-out [6–7]) that results in an effective increase in the cluster radius which was not taken into account before. These predictions have been nicely confirmed by recent experiments on small sodium and potassium clusters [16], which show that the polarisability is in fact 60% to 80% higher than R^3 and slowly converges towards the bulk (classical) value.

The physically more relevant description of the electronic cloud is achieved in the context of the density functional theory (DFT) [17, 18]. The static electric polarisability

0953-8984/89/5110391 + 15 $02.50

is then obtained from the linear response theory [19, 20] within the DFT. Recently [21], we have obtained the m_1 and m_3 moments of the random phase approximation (RPA) strength function corresponding to multipole operators and have applied them to the study of surface collective oscillations.

The purpose of the present work is to complete this study by obtaining the electric polarisability, which is closely related to the m_{-1} moment of the strength. We have considered only Na and Ag clusters made of up to $N = 1000$ atoms and multipolarities $L \leqslant 15$. However, our method is fast and numerically reliable for larger values of N and L. It can also be used for other metallic materials provided the following basic hypotheses apply:

(i) the valence-electron cloud of the unperturbed cluster is described within the spherical jellium model (SJM) and a Thomas–Fermi–Weizsäcker plus a local density approximation (LDA) (Dirac+Wigner) for exchange–correlation effects;

(ii) the external field acts only on the valence electrons.

As these hypotheses are currently used in semiclassical calculations of metal clusters *and* metal spheres, the method we use in this work applies to both systems, which will be referred to as clusters.

The paper is organised as follows: sum rules are defined in § 2, where we present a summary of the fundamental results of this technique and derive the main formulae that will be used in § 3 to obtain the numerical results. Finally, we draw our conclusions in § 4.

2. Sum rules

2.1. General description

Sum rules are moments of the strength function

$$S(E) = \sum_n \delta(E - E_n)\,|\langle n|Q|\varphi\rangle|^2 \tag{1}$$

where the sum (integral in the case of continuum spectrum) extends over all the excited states of the system. Q is the external field acting on the system and E_n, $|n\rangle$ and $|\varphi\rangle$ are the excitation energies, the excited states and the ground state (GS) of the system, respectively. The kth-order moment is defined as

$$m_k = \int \mathrm{d}E\, E^k S(E) = \sum_n E_n^k |\langle n|Q|\varphi\rangle|^2. \tag{2}$$

From these moments, the average energy and variance of the strength can be obtained:

$$\begin{aligned} \bar{E} &= m_1/m_0 \\ \sigma^2 &= m_2/m_0 - m_1^2/m_0^2. \end{aligned} \tag{3}$$

A direct computation of m_k from equation (2) is hopeless in most practical cases because one should know the whole spectrum. However, *odd* moments of $S(E)$ can be obtained with RPA precision as expectation values of suitable operators on the Hartree–Fock (HF) (or Kohn–Sham (KS) in the present context) *ground state* $|\varphi\rangle$.

Defining the 'mean energies' $E_k = (m_k/m_{k-2})^{1/2}$, it has been shown [22] that

$$\begin{aligned} E_1 &\leqslant \bar{E} \leqslant E_3 \\ \sigma^2 &\leqslant (E_3^2 - E_1^2)/4. \end{aligned} \tag{4}$$

These equations allow one to estimate the centroid $\bar{E}$ and variance σ^2 of $S(E)$ by

evaluating just three moments, m_{-1}, m_1 and m_3. If most of the strength is concentrated in a narrow energy region, as it is for some resonance states, then E_1 and E_3 are estimates of $\bar{E}$. Conversely, whenever E_1 and E_3 are close we may infer that an appreciable part of the strength is concentrated around these values and that the response of the system to the operator Q is dominated by the resonance-state contribution.

For m_1 and m_3 we have [22, 23]:

$$\begin{aligned} m_1 &= \tfrac{1}{2}\langle\varphi|[Q,[H,Q]]|\varphi\rangle \\ m_3 &= \tfrac{1}{2}\langle\varphi|[[H,[H,Q]],[H,Q]]|\varphi\rangle. \end{aligned} \tag{5}$$

m_1 is straightforwardly evaluated from the first of equations (5). m_3 is determined more easily by scaling the Slater determinant $|\varphi\rangle$ obtained by solving the KS equations for the unperturbed cluster. Indeed, defining the scaled wavefunction (WF)

$$|\varphi_\eta\rangle = \mathrm{e}^{\eta[H,Q]}|\varphi\rangle \tag{6}$$

we get

$$m_3 = \tfrac{1}{2}(\partial^2/\partial\eta^2)\langle\varphi_\eta|H|\varphi_\eta\rangle|_{\eta=0}. \tag{7}$$

It has been shown [22] that equations (5) give m_1 and m_3 *with RPA precision* if they are evaluated using the GS KS WF $|\varphi\rangle$ corresponding to the Hamiltonian H.

The inverse energy-weighted sum rule

$$m_{-1} = \sum_n \frac{1}{E_n}|\langle n|Q|\varphi\rangle|^2 \tag{8}$$

is closely related to the static polarisability α:

$$\alpha = 2m_{-1}. \tag{9}$$

The static polarisability has been obtained for the dipole operator and other multipole operators in the RPA approximation from the RPA response function at zero energy [8, 10], and also from the so called modified Sternheimer equation [7], which is equivalent to the RPA calculation. It is also possible to get α with RPA precision from constrained HF (or KS) calculations. Indeed, solving the constrained problem

$$H + \lambda Q \tag{10}$$

in the HF (KS) approximation, where λ is a small constraining parameter, it is possible to show [24] that m_{-1} RPA can be obtained as

$$m_{-1} = -\tfrac{1}{2}(\mathrm{d}\langle Q\rangle_\lambda/\mathrm{d}\lambda)|_{\lambda=0} = \tfrac{1}{2}(\mathrm{d}^2\langle H\rangle_\lambda/\mathrm{d}\lambda^2)|_{\lambda=0}. \tag{11}$$

In almost all cases of practical interest, to solve the constrained HF (CHF) problem is a formidable task because the external field breaks the spherical symmetry of the unperturbed cluster. Only for the $L = 0$ volume mode for which Q is chosen as r^2 or the spherical zeroth-order Bessel function $j_0(qr)$, the Euler–Lagrange equations associated with equation (10) are easy to solve (see reference [21] for the case $Q = r^2$).

Fortunately, the possibility of evaluating m_{-1} (thus α) via a static constrained calculation justifies the applicability of approximated methods based on the hypothesis of local equilibrium [25], like the semiclassical Thomas–Fermi (TF) method. Loosely speaking, m_{-1} characterises the hydrodynamical or adiabatic response of the system to an external field, whereas m_3 does it for the elastic or sudden response [9].

The self-consistent (trial function density or fully variational) TF model has lent itself to evaluate m_{-1} for a large class of constraining operators in nuclear physics (see

reference [23] for a review, and references therein). In the field of metallic clusters, it has been used by Snider and Sorbello to study the dipole polarisability with some success [6]. We shall show in the following sections that, when used properly, the method yields results comparable to full RPA calculations [26] for moderately high multipolarities.

2.2. m_1 and m_3 for the multipole operator $r^L Y_{L0}$

It is possible to show [21] (see also reference [14]) that

$$m_1 = \frac{\hbar^2}{2m} L(2L+1) \int_0^\infty \mathrm{d}r\, r^{2L} n_0(r) \tag{12}$$

where $n_0(r)$ is the unperturbed GS electronic density and m the electron mass.

The m_3 sum rule consists of three terms [21, 14], one ($m_3(T)$) coming from the kinetic energy and two from the electron–electron Coulomb energy (m_3(e–e)) and the jellium–electron Coulomb energy (m_3(j–e)). In the TF approximation (see reference [21] for a thorough discussion) they read:

$$m_3(T) = \left(\frac{\hbar^2}{m}\right)^2 \tfrac{2}{3} L(2L+1)(L-1)(2L-1) \int_0^\infty \mathrm{d}r\, r^{(2L-2)} \frac{\hbar^2}{2m} \tau_0(r) \tag{13}$$

$$m_3(\text{e–e}) = -e^2 \left(\frac{\hbar^2}{m}\right)^2 L^2(L-1) \int_0^\infty \mathrm{d}r\, n_0(r) r^{(2L-3)} \int_0^r \mathrm{d}r_1 n_0(r_1) \tag{14}$$

$$m_3(\text{j–e}) = -2\pi e^2 \left(\frac{\hbar^2}{m}\right)^2 L^2 \int_0^\infty \mathrm{d}r\, r^{(2L-2)} n_0'(r) \int_0^r \mathrm{d}r_1 r_1^2 n_j(r_1) \tag{15}$$

where $n_0'(r)$ denotes the GS unperturbed electronic density r-derivative and n_j the constant jellium density

$$n_j(r) = n^+ \Theta(R - r) \tag{16}$$

with $R = r_s N^{1/3}$, r_s being the radius per valence electron of the bulk monovalent metal, N the number of atoms in the cluster (i.e., the cluster number) and n^+ the positive background density, $n^+ = 3/(4\pi r_s^3)$. The unperturbed kinetic energy density reads:

$$\tau_0(r) = \tfrac{3}{5}(3\pi^2)^{2/3} n_0^{5/3}(r) + (\beta/4)(\nabla n_0(r))^2 / n_0(r). \tag{17}$$

The second-order gradient term is the exact kinetic energy density for a one-electron system if $\beta = 1$. Snider and Sorbello have used $\beta = 1/9$ which is the Kirzhnits value [27], as well as 2/9. We have taken β as a free parameter which we have fixed in order to reproduce the E_3 RPA energy on average.

Figure 1 shows the E_3 energies (in atomic units, i.e. $\hbar = m = e^2 = 1$, energy unit = 27.2 eV, length unit = 0.529 Å) for different Na clusters. The full triangles correspond to the RPA calculations whereas the full curves show the TF calculation with an effective β. Figure 2 shows the E_3 energies corresponding to Ag. A more careful analysis than that made in reference [21] has led us to take $\beta = 0.50$ for Na and $\beta = 0.40$ for Ag as optimum values. We shall use these values as well as r_s(Na) = 4 and r_s(Ag) = 3 (in au) to obtain the multipole polarisabilities in the next sections. For the sake of completeness, we also show in these figures the results for the $L = 0$ volume mode, which is actually not considered in the present study.

2.3. m_{-1} for the multipole operator $r^L Y_{L0}$

To obtain m_{-1}, we have to solve the constrained problem

$$E[n] = \int \mathrm{d}r\, \varepsilon(n) + \lambda \int Q n(r)\, \mathrm{d}r \tag{18}$$

where $Q = r^L Y_{L0}$ and λ is a *small* parameter. The energy density functional $\varepsilon(n)$ is the

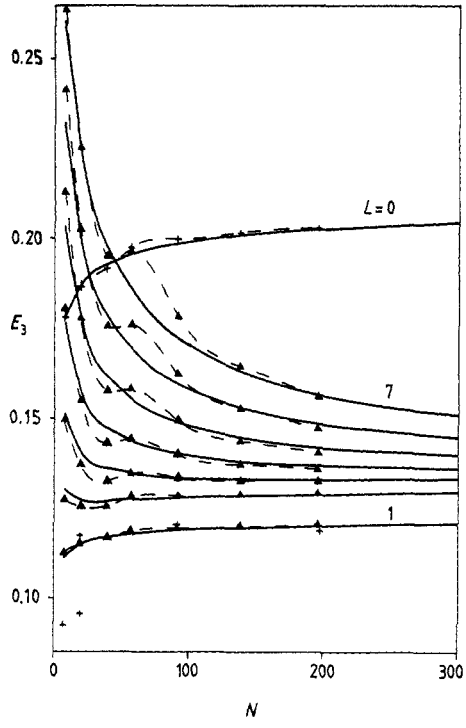

Figure 1. E_3 energies (in au) for Na clusters. From bottom to top the curves correspond to $L = 1$ to 7, and to $L = 0$ (upper curve and crosses). The full triangles correspond to the KS-RPA calculation and the full curves to the TFDW calculation. The broken curves are only to guide the eye. The crosses near the $L = 1$ curve are the results of reference [9]. The two crosses near the bottom corner are experimental results from references [36] and [37].

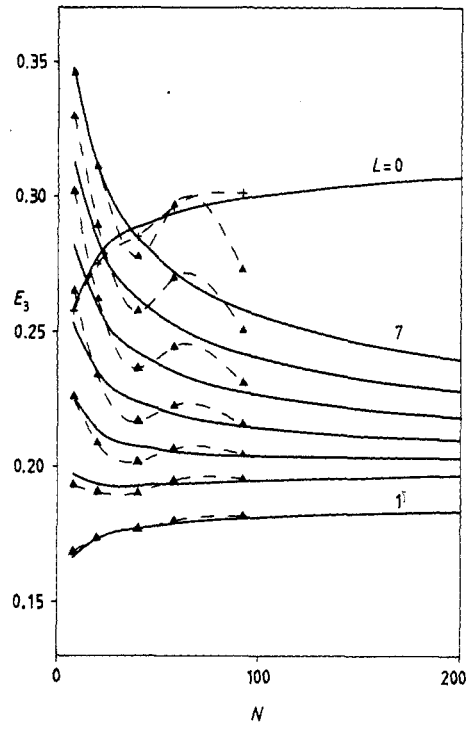

Figure 2. As figure 1 but for Ag clusters.

same we have used in reference [21] and also that of reference [6], apart from the Weizsäcker coefficient, as mentioned in § 2.2. In atomic units, it reads

$$\varepsilon(n) = \tfrac{1}{2}\gamma n^{5/3} + \tfrac{1}{8}\beta\frac{(\nabla n)^2}{n} - C_x n^{4/3} - \frac{an}{b+(3/4\pi n)^{1/3}} + \tfrac{1}{2}\int\frac{n(\boldsymbol{r})n(\boldsymbol{r}')}{|\bar{\boldsymbol{r}}-\bar{\boldsymbol{r}}'|}\,\mathrm{d}\boldsymbol{r} + V_j n \tag{19}$$

where $\gamma = 3/5(3\pi^2)^{2/3}$, $C_x = 3/4(3/\pi)^{1/3}$, $a \simeq 0.44$, $b = 7.8$ and V_j is the Coulomb potential created by the jellium:

$$V_j = \begin{cases}(2\pi/3)n^+r^2 - 2\pi R^2 n^+ & r \leqslant R\\ -N/r = -(4\pi/3)R^3 n^+/r & r \geqslant R.\end{cases} \tag{20}$$

In order to find the equilibrium density $n(\boldsymbol{r})$, one has to solve the Euler–Lagrange equation

$$\delta\varepsilon(n)/\delta n + \lambda r^L Y_{L0} = \mu_\lambda \tag{21}$$

where μ_λ is the chemical potential. Since we are interested only in λ^1-order changes in $n(\boldsymbol{r})$ with respect to the unconstrained equilibrium density $n_0(r)$ (see equation (11)), we can write without loss of generality

$$n(\boldsymbol{r}) = n_0(r) + \delta n(\boldsymbol{r}) \equiv n_0(r) + \lambda f(r) Y_{L0} \tag{22}$$

with $f(r)$ an arbitrary function of r that depends on L. Integrating equation (22) over $\mathrm{d}\boldsymbol{r}$, one easily sees that $n(\boldsymbol{r})$ is properly normalised to first order in λ. Thus, one can replace in equation (21) μ_λ by the $\lambda = 0$ chemical potential μ. Substituting equation (22) into equation (21) and using the equilibrium condition at $\lambda = 0$

$$\delta\varepsilon(n_0)/\delta n_0 = \mu$$

we get the following integro-differential equation for $f(r)$:

$$\begin{aligned} -\frac{\beta}{4}\frac{\mathrm{d}^2 f}{\mathrm{d}r^2} + \frac{\beta}{4}\left(-\frac{2}{r} + \frac{n_0'}{n_0}\right)\frac{\mathrm{d}f}{\mathrm{d}r} + \left\{\frac{\beta}{4}\left[\frac{L(L+1)}{r^2} + \frac{\Delta n_0}{n_0} - \left(\frac{n_0'}{n_0}\right)^2\right]\right. \\ \left. + \tfrac{5}{9}\gamma n_0^{2/3} - \tfrac{4}{9}C_x n_0^{1/3} - \tfrac{2}{9}a r_s(n_0)\frac{[b + 2r_s(n_0)]}{[b + r_s(n_0)]^3}\right\} f + n_0 r^L \\ + \frac{4\pi}{2L+1}\left(\frac{n_0}{r^{(L+1)}}\int_0^r \mathrm{d}r_1 r_1^{(L+2)} f(r_1) + n_0 r^L \int_r^\infty \mathrm{d}r_1 \frac{f(r_1)}{r_1^{(L-1)}}\right) = 0. \end{aligned} \tag{23}$$

In equation (23), $n_0'(r)$ denotes the r-derivative of the (spherical) equilibrium density $n_0(r)$, and $r_s(n_0) = (4\pi n_0/3)^{-1/3}$ is the *local* radius per electron. It is worth noting that the differential character of equation (23) arises from the Weizsäcker correction. Had we taken $\beta = 0$, we would have ended up with a much simpler integral equation, as is the case in references [4] and [15]. After determining the induced radial density $f(r)$ we have

$$\langle Q\rangle_\lambda = \int \mathrm{d}\boldsymbol{r}\, r^L Y_{L0} n(\boldsymbol{r}) = \int \mathrm{d}\boldsymbol{r}\, r^L Y_{L0}\delta n(\boldsymbol{r}).$$

Thus

$$\alpha = 2m_{-1} = -\int_0^\infty \mathrm{d}r\, r^{(L+2)} f(r). \tag{24}$$

Consequently, to obtain the static polarisability within this method, one has to solve an integro-differential equation and perform an integral. This is much simpler than solving the CHF problem (equation (10)) and carrying out a delicate numerical derivative with respect to the small parameter λ (see equation (11)).

Before we present the results corresponding to the exact solution to equation (23), let us discuss two limiting cases. First notice that neglecting kinetic, exchange and correlation contributions we recover the classical limit. The resulting integral equation

$$R^L + \frac{4\pi}{2L+1}\left(\frac{1}{R^{(L+1)}}\int_0^R \mathrm{d}r\, r^{(L+2)} f(r) + R^L \int_R^\infty \mathrm{d}r \frac{f(r)}{r^{(L-1)}}\right) = 0 \tag{25}$$

has solutions of the kind

$$f(r) = A\delta(r - R). \tag{26}$$

Upon substitution into equation (25) one finds:

$$A = -[(2L+1)/4\pi]R^{(L-1)} \tag{27}$$

and from equation (24),

$$\alpha_{\mathrm{Cl}} = [(2L+1)/4\pi]R^{(2L+1)} \tag{28}$$

which is the classical result (the coefficient in front of $R^{(2L+1)}$ comes from the spherical

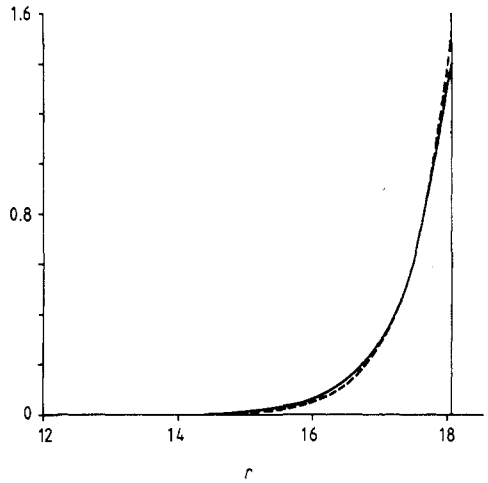

Figure 3. Na_{92} normalised induced electron densities $r^2f(r)$ obtained from the constant-electron-density model. Full curve, $L = 1$; broken curve, $L = 10$.

harmonic Y_{L0}). One can also arrive at this result from the surface oscillations of a charged incompressible and irrotational liquid drop, a well known model in nuclear physics (see, e.g., appendix 6A of reference [28]).

The next step in complexity is to consider the electron density as constant up to the jellium surface. This is basically the model of reference [4], which yields polarisabilities smaller than the classical value. In this case equation (23) becomes again an integral equation that could be solved analytically (see reference [4]) but that we have solved numerically using the same technique applied in the integro-differential case. Following reference [26], we have normalised $f(r)$ as follows:

$$\int_0^\infty dr\, r^2 f(r) = 1. \tag{29}$$

In figure 3 we have drawn the quantity $r^2f(r)$ corresponding to the Na_{92} cluster for $L = 1$ and $L = 10$. The crudeness of this model will be more apparent when we present in the next subsection the solutions corresponding to the Thomas–Fermi–Dirac–Weizsäcker (TFDW) electronic density.

3. Results

3.1. Full variational results

Equation (23) has been solved by standard matrix analysis techniques, after discretising it by using three-point formulae for the $n_0(r)$ and $f(r)$ r-derivatives and the trapezoidal rule to perform the Coulomb integrals. We have imposed the boundary conditions $f(\infty) = 0$ and $f(0) = 0$, the latter one in order to have $\delta n(r)$ well defined at $r = 0$.

Figures 4 and 5 show $r^2f(r)$ normalised to unity, corresponding to Ag_{20} and Na_{20}. The vertical lines indicate the position of the jellium surface. The sizeable spill-out of the electron-induced density is clearly manifested in these figures. These induced densities are in qualitative agreement with those obtained by Ekardt [26] in a full RPA calculation.

We have found that the position of the induced density peak depends little on L for small values of L. Actually, for a given N-cluster, the peak moves inwards when L increases from $L = 1$ up to a certain L_{max} which depends on N. From L_{max} on, the peak moves outwards and for $L \gg L_{max}$, it will eventually lay much farther away from R than the $L = 1$ peak. This is at variance with the findings of reference [26]. We shall come back to this point when we discuss tables 1 and 2 in the next subsection.

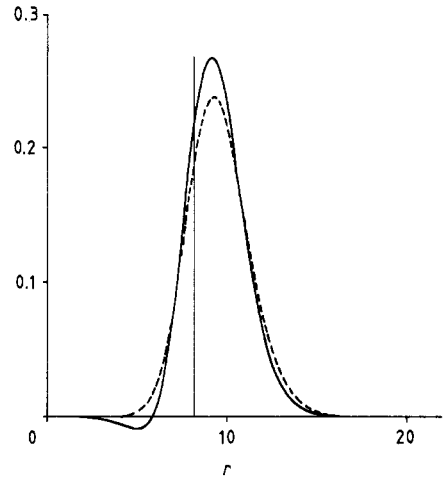

Figure 4. Ag_{20} normalised induced electron densities $r^2 f(r)$ obtained from equation (23). Full curve, $L = 1$; broken curve, $L = 5$.

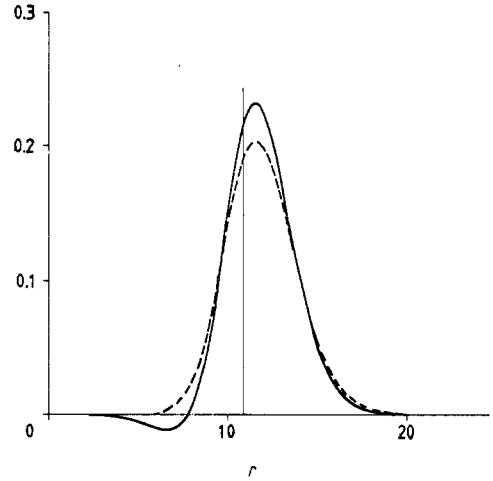

Figure 5. As figure 4 but for Na_{20}.

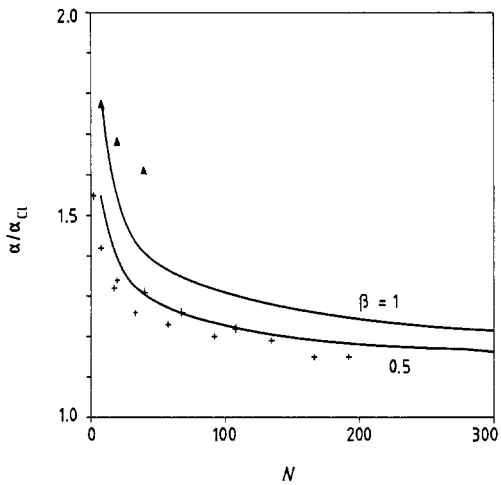

Figure 6. Dipole polarisabilities for Na clusters obtained with two different values of the Weizsäcker coefficient β for $L = 1$. The crosses are the RPA results of reference [8] and the triangles the experimental values of reference [16], as quoted in reference [15].

It is interesting to note that, apart from a sizeable shift outwards, $r^2 f(r)$ look very much as $-r^2 n_0'(r)$ (see, e.g., figures 1 and 2 of reference [21]). This is what one might expect to find as the most natural generalisation of the classical induced density, equation (26).

Figure 6 displays the dipole polarisability of Na clusters in units of the classical value α_{Cl}. The crosses correspond to the RPA results of Ekardt [8], and the triangles to the experimental values of reference [16]. The results obtained from equation (23) are the curve labelled $\beta = 0.5$.

To see how the chosen β influences the polarisability value, we have also drawn the results corresponding to $\beta = 1$. The increase of the polarisability with β is not surprising, since this parameter acts on the surface diffuseness and exponential fall-off of the electronic density [21]. This makes clear the interest of looking at other moments of the $S(E)$ when one studies the polarisability with phenomenological models. Actually, since our energy density functional is similar to that of reference [8], one should not expect *real* improvements on the results obtained there. We attribute the minor differences

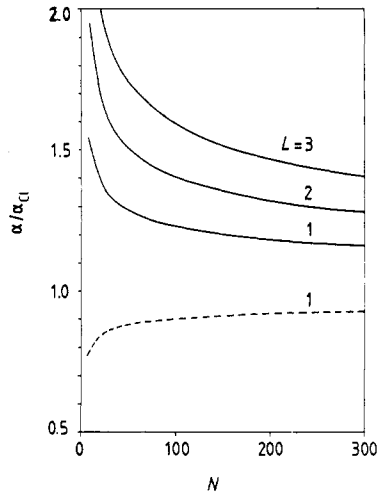

Figure 7. Na static polarisabilities for $L = 1$ to 3 (full curves). The broken curve corresponds to the $L = 1$ polarisability obtained from the constant-electron-density model.

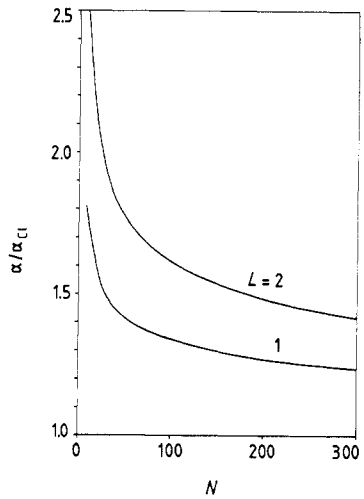

Figure 8. Ag static polarisabilities corresponding to $L = 1$ and 2.

between the results of both calculations to the different correlation energy we use and, mainly, to the different fall-off of TF and KS densities. The same comment applies to the results obtained in reference [14].

Figure 7 shows the $L = 1, 2$ and 3 static polarisabilities of Na clusters. Each polarisability has been normalised to its classical value, equation (28). Also shown in this figure is the dipole polarisability corresponding to the constant electron density (broken curve). The lack of spill-out in the induced density results in a value of α below α_{Cl}, this effect being more sizeable for small clusters in which the surface-to-volume ratio is larger than in big clusters. Analogously, figure 8 shows the $L = 1$ and 2 polarisabilities of Ag clusters.

Figure 9 displays the evolution with N of the E_1 and E_3 energies in the case of Na clusters for $L = 1, 2$ and 5. Several interesting features show up. First, notice that the variance of $S(E)$, estimated by

$$\sigma^2 \sim (E_3^2 - E_1^2)/4 \tag{30}$$

increases with increasing L, meaning that for a given cluster, the bigger the multipolarity, the lesser collective the mode. This behaviour is especially marked for small clusters. Equivalently, σ^2 decreases with N for a given L, indicating that big clusters can sustain surface collective oscillations of higher multipolarity than small clusters.

It is also interesting to consider the limit of $E_3(L)$ and $E_1(L)$ when N goes to infinity. We have shown in reference [21] that for a constant electron density (see also reference [14])

$$m_1 = (\hbar^2/2m)n_0 L R^{(2L+1)} \tag{31}$$

$$m_3 = (\hbar^2/m)^3 \tfrac{1}{3} L(2L+1)(L-1)\gamma n_0^{5/3} R^{(2L-1)} + 2\pi e^2 (\hbar^2/m)^2 n_0^2 R^{(2L+1)} L^2/(2L+1) \tag{32}$$

with $n_0 = n^+$. Thus, when R (i.e., N) goes to infinity we recover Mie's classical result:

$$E_3^2(L) = \hbar^2 \omega_p^2 L/(2L+1) \tag{33}$$

where $\omega_p^2 = 4\pi n_0 e^2/m$.

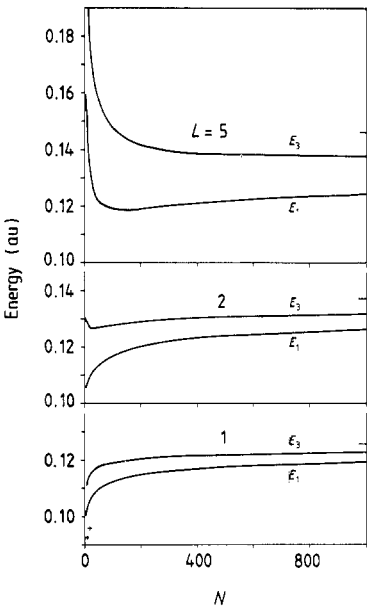

Figure 9. E_1 and E_3 energies (in au) for Na clusters and $L = 1, 2$ and 5. As in figure 1, the two crosses represent experimental results.

In the classical limit, we have from equation (28) that

$$m_{-1} = \tfrac{1}{2}\alpha = [(2L + 1)/8\pi e^2]R^{(2L+1)}. \tag{34}$$

Combining equations (31) and (34), when $N \to \infty$ we get:

$$E_1^2(L) = \hbar^2\omega_p^2 L/(2L + 1) \tag{35}$$

which is precisely $E_3^2(L)$. Consequently, in this limit we obtain again the surface plasmon energy $E_p(L)$ and have $\sigma^2 = 0$. $E_p(L)$ is indicated at the right-hand edge of each part of figure 9 by a short horizontal trace. For high values of L and small clusters, E_3 and E_1 are blue-shifted with respect to E_p, but when N increases, E_1 and E_3 tend to $E_p(L)$ from below. As an example, for the Na_{1000} cluster we have found $E_1 = 0.119$ and $E_3 = 0.122$ for $L = 1$, whereas the classical limit is $E_p = 0.125$ (in atomic units).

Following references [6] and [26], we have introduced a distance δ such that

$$\alpha/\alpha_{Cl} = (1 + \delta/R)^{(2L+1)}. \tag{36}$$

Since $\alpha > \alpha_{Cl}$, δ is a positive quantity. When $L = 1$, in the limit $R \to \infty$ it gives the location δ_p of the image plane [29] with respect to the jellium surface. For the Na_{1000} cluster we have found $\delta = 1.40$, in agreement with the Lang–Kohn value $\delta_p = 1.3 \pm 0.2$ [29]. We have also found $\delta = 1.25$ for Na_8, 1.33 for Na_{92}, 1.37 for Na_{300} and 1.38 for Na_{500}, all compatible with the above δ_p. It seems, however, that these values point to a δ_p slightly bigger than 1.40.

3.2. Trial function calculations

Although the solution of equation (23) turns out to be rather easy, it is desirable to make use of a much simpler, yet reliable method to obtain α. A standard procedure consists of expanding equation (18) up to terms in λ^2 using equations (19) and (22), and then minimising $E[n]$ by means of a trial function $f(r)$ which depends on a few parameters [6]. After a straightforward calculation we get

$$\frac{E[n] - E[n_0]}{\lambda^2} \equiv \frac{\delta E}{\lambda^2} = \int_0^\infty \mathrm{d}r\, r^2 \left\{ f^2(r) \left[\tfrac{5}{18}\gamma n_0^{-1/3} - \tfrac{2}{9}C_x n_0^{-2/3} - \tfrac{1}{9}a r_s(n_0) \frac{(b + 2r_s(n_0))}{n_0(b + r_s(n_0))^3} + \tfrac{1}{8}\frac{\beta}{n_0}\left(\frac{n_0'}{n_0}\right)^2 \right] \right.$$

Table 1. Na_{92} static polarisability α/α_{Cl} and δ parameter (in au) defined in equation (36) for $L = 1$ to 15. The row labelled 'variational' corresponds to the exact solution to equation (23). The rows labelled 2P and 4P are trial function results obtained with two and four parameters respectively (see equation (38)). The entry SEFR is the value of Sorbello's electrostatic force rule, equation (39).

Na_{92}	Variational		2P		4P	
L	α/α_{Cl}	δ	α/α_{Cl}	δ	α/α_{Cl}	δ
1	1.24	1.33	1.23	1.30	1.24	1.33
2	1.42	1.31	1.40	1.26	1.41	1.29
3	1.61	1.27	1.59	1.23	1.60	1.26
4	1.81	1.24	1.76	1.16	1.80	1.21
5	2.03	1.20	1.96	1.14	2.01	1.18
6	2.25	1.17	2.15	1.10	2.21	1.14
7	2.52	1.15	2.36	1.06	2.44	1.11
8	2.85	1.15	2.62	1.05	2.73	1.10
9	3.30	1.17	2.97	1.07	3.10	1.11
10	3.97	1.22	3.48	1.11	3.64	1.15
11	5.01	1.31	4.25	1.17	4.47	1.21
12	6.72	1.43	5.49	1.27	5.75	1.31
13	9.68	1.58	7.54	1.40	7.91	1.44
14	15.1	1.77	11.2	1.57	11.8	1.60
15	25.8	2.00	18.1	1.77	19.0	1.80
SEFR	1.0000		0.9885		0.9937	

$$-\tfrac{1}{4}\beta\frac{n_0'}{n_0^2}f(r)f'(r)+\tfrac{1}{8}\beta\frac{f'^2(r)}{n_0}+r^L f(r)\Big\}+\tfrac{1}{8}\beta L(L+1)$$
$$\times\int_0^\infty \mathrm{d}r\frac{f^2(r)}{n_0}+\frac{4\pi}{2L+1}\int_0^\infty \mathrm{d}r f(r)\frac{1}{r^{(L-1)}}\int_0^r \mathrm{d}r_1 r_1^{(L+2)}f(r_1). \tag{37}$$

This equation is the generalisation of equation (9) of reference [6] for any multipolarity L. Obviously, a fully variational determination of $f(r)$ from equation (37) is completely equivalent to solving the Euler–Lagrange equation (23). We have verified numerically this point because it constitutes a test of the numerical method. Indeed, it is apparent from equation (11) that the right-hand side of equation (37) yields m_{-1} for the function $f(r)$ that minimises $E[n]$ expanded up to λ^2. We have checked that when we substitute into equation (37) the function $f(r)$ solution of equation (23), we get a value of $\alpha = 2m_{-1}$ that coincides with the values shown in the previous subsection within ~0.1%, which sets the limit of our numerical accuracy.

In practice, the usefulness of equation (37) is to furnish α by minimising $\delta E/\lambda^2$ employing a trial function $f(r; p_i)$ which depends on a few parameters p_i, $i = 1, \ldots, m$. Guided by figures 4 and 5, a natural guess for $f(r; p_i)$ is

$$f(r; p_i) = (p_2 + p_3 r + p_4 r^2)\, n_0'(r + p_1) \tag{38}$$

i.e., a polynomial times the r-derivative of the variational unperturbed density n_0 (easily available from variational TFDW calculations) *shifted* a certain amount p_1. This shift is a basic ingredient if one wants to reproduce the full variational results. For instance, p_1 and p_2 are enough to recover the Na_{92} variational results for $L = 1$ to 5 within ~3%. That can be seen in table 1, where we have collected the exact, two-parameter (2P) and four-parameter (4P) results for $L = 1$ to 15 corresponding to Na_{92}. Table 2 collects the exact and 4P results for Na_{20} up to $L = 10$.

Table 2. As table 1 but for Na_{20} up to $L = 10$.

Na_{20}	Variational		4P	
L	α/α_{Cl}	δ	α/α_{Cl}	δ
1	1.40	1.28	1.40	1.28
2	1.70	1.22	1.70	1.22
3	2.01	1.14	2.01	1.14
4	2.35	1.08	2.33	1.07
5	2.79	1.06	2.74	1.04
6	3.50	1.10	3.36	1.06
7	4.83	1.20	4.50	1.15
8	7.56	1.37	6.77	1.29
9	13.6	1.60	11.7	1.50
10	28.6	1.88	23.3	1.76
SEFR	0.9997		0.9958	

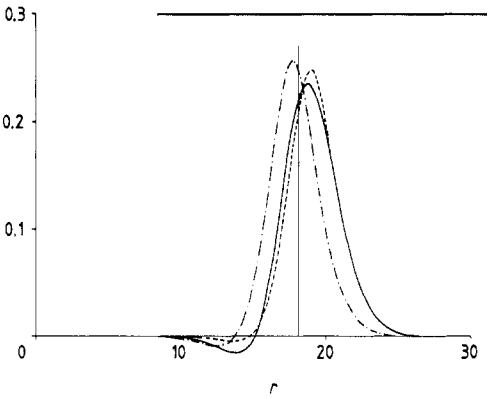

Figure 10. Na_{92} normalised induced electron density $r^2f(r)$ for $L = 1$ obtained from equation (23) (full curve) and from equation (37) (broken curve). The chain curve corresponds to the normalised $r^2n_0'(r)$.

In figure 10 we compare the normalised $r^2f(r)$ induced variational density (full curve) and the 4P induced trial density (broken curve) corresponding to Na_{92} and $L = 1$. Notice that both densities coincide for large r. This is the reason for the excellent agreement between both calculations (see equation (24)). We also show the normalised $r^2n_0'(r)$ (chain curve). Notice the key role played by the shifting parameter p_1 introduced in equation (38). Indeed, trial functions of the kind $p_2n_0'(r)$ yield $\alpha/\alpha_{Cl} = 1.18$ for Na_{20} and 1.10 for Na_{92} in the dipole case.

We have checked that our $L = 1$ results fulfil Sorbello's electrostatic force rule (SEFR) with high accuracy. This rule states that for $L = 1$ [30]

$$-\frac{4\pi}{3}\left(\frac{1}{R^3}\int_0^R \mathrm{d}r\, r^3 f(r) + \int_R^\infty \mathrm{d}r\, f(r)\right) = 1. \tag{39}$$

One can see from tables 1 and 2 that this rule, indicated by the entry SEFR, is verified very well for the variational density and also for the 4P and 2P trial densities.

Within the trial function procedure, one may take advantage of the fact that m_{-1} can be obtained in two independent ways (see equation (11)), either directly from equation (37) or using equation (24), to carry out another test on the numerical method. However, we would like to emphasise that, in contrast to what is stated in reference [6], this test *only* concerns the minimisation routine and *not* the adequacy of the trial function $f(r)$. This is obvious if one realises that the equalities (11) hold only for the *equilibrium* (i.e. minimum) solution of the constrained problem equation (18). This minimum solution

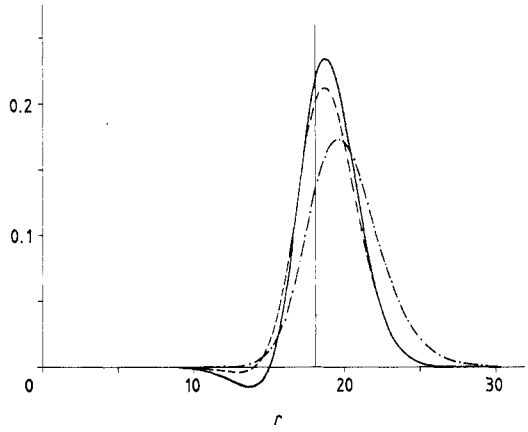

Figure 11. Na_{92} normalised induced electron densities $r^2f(r)$ obtained from equation (23). Full curve, $L = 1$; broken curve, $L = 6$; chain curve, $L = 15$.

might well be obtained within a class of poor trial densities. As an example, consider the 1P trial density $p_2 n_0'(r)$, for which the minimisation of equation (37) can be carried out analytically because $\delta E/\lambda^2$ is parabolic in p_2. Both ways of obtaining m_{-1} yield the same result since the calculation is consistent and numerically exact, but the polarisability is wrong. In our 2P and 4P calculations, the polarisabilities obtained with either formula agree to better than 0.5%, for $L \leqslant 5$.

Finally, we would like to comment on the non-monotonic behaviour of δ with L shown in tables 1 and 2. As Ekardt pointed out [26], δ seems to decrease when L increases (for Na_{92}, up to $L \sim 8$ in our model and up to $L \sim 10$ in reference [26]). However, above some value of L we have found that δ increases rapidly, as well as α/α_{Cl}. To check that this is not a numerical artifact, we have increased the radius of the sphere in which the calculations have been performed and have also used in equation (23) the KS $n_0(r)$ density, which has a different fall-off than the TFDW density. In both cases, we have found the same qualitative behaviour of $\delta(L)$.

We show in figure 11 $r^2f(r)$ for Na_{92} corresponding to $L = 1$, 6 and 15. From this figure, it is clear that the origin of the increase of δ is twofold: the $r^2f(r)$ peak moving outwards and its spreading. These facts should be contrasted with RPA calculations performed for values of L higher than those of reference [26].

It is worth mentioning that, for a given cluster, the response at increasingly higher values of L is not classical at all and is eventually dominated by electron–hole contributions of non-collective character [26, 21]. Consequently, our TFDW calculation can only furnish qualitative results for these high multipole polarisabilities.

4. Summary and outlook

In this paper we have thoroughly studied the static multipole polarisability of small metallic clusters in a TFDW approximation. It has led us to an integro-differential equation for the induced electronic density that we have solved self-consistently using the TFDW electronic density of the unperturbed spherical cluster. By suitable simplifications of that equation, the classical and constant electronic density results are recovered.

Besides the polarisability, we have also studied other moments of the strength function from which we have defined two average energies and estimated the width of the surface mode for different multipolarities. We have found that the width of the resonance increases rapidly when L increases, this effect being more marked for small clusters and big values of L.

For Na clusters, for which the jellium model is adequate, we have obtained an N-dependence of the dipole resonance energy that compares well with very recent experimental results [31]. This is not quite so for Ag clusters [32]. The discrepancy is attributed to the role played by the Ag d electrons (see reference [32] for a thorough discussion of this effect).

To circumvent the solution of the integro-differential equation, we have minimised the constrained energy using a trial function procedure. This method basically yields the same results as the exact solution to that equation for small values of L, which are the physically more relevant.

Our results agree with detailed RPA calculations on average. The simplicity of our self-consistent method has allowed us to test the influence on the polarisability of the unperturbed electronic density. Using different values of the effective Weizsäcker coefficient, we have shown that α depends appreciably on the unperturbed density profile (see also reference [6]).

Despite a qualitative agreement, the dipole polarisability obtained in the present calculation and in other calculations quoted herein, is still lower than experiment by about 20%. To improve it, some attempts have been made to go beyond SJM by taking into account the ionic structure [11]. However, averaged over all orientations of the cluster, the polarisability results are analogous to those of the SJM. Another effect associated with the jellium background, namely its elastic deformation due to the external polarising field, increases the dipole polarisability by only about 1% [12]. Some morphological changes in the jellium density, like an effective surface diffuseness, would also increase the polarisability, since it increases the electron spill-out [33].

The major part of the discrepancy between theoretical and experimental results has thus been attributed to the LDA to the exchange–correlation energy in DFT [13]. The self-interaction correction (SIC) [34] to the LDA reduces the disagreement from ~20% to ~10%. This is so because the SIC–LDA method yields a better energy-level structure than the LDA [34], influencing the RPA polarisability results as stressed by Ekardt and Penzar [35]. Indeed, the SIC-LDA method improves the asymptotic behaviour of the LDA exchange–correlation potential, leading to better single-electron wavefunctions. The improvements of the SIC can be incorporated in our KS [21] and TFDW method. Work along these lines is in progress.

Acknowledgments

We are indebted to Nuria Barberán and Joao P. da Providencia for useful discussions. This work has been supported by the CICYT (Spain) Grants PB85-0072-C02, PB86-0654-C02 and AE82-0027, by the University of Valencia-University of the Balearic Islands exchange programme and by the Junta de Castilla-León.

References

[1] de Heer W A, Knight W D, Chou M Y and Cohen M L 1987 *Solid State Physics* vol **40** ed. H Ehrenreich and D Turnbull (New York: Academic) p 93

[2] Rice M J, Schneider W R and Strässler S 1973 *Phys. Rev.* B **8** 474

[3] Dasgupta B and Fuchs R 1981 *Phys. Rev.* B **24** 554

[4] Lushnikov A A, Maksimenko V V and Simonov A J 1982 *Electromagnetic Surface Modes* ed. A D Boardman (New York: Wiley) p 305

[5] Ekardt W, Tran Thoai D B, Frank F and Shulze W 1983 *Solid State Commun.* **46** 571
[6] Snider D R and Sorbello R S 1983 *Phys. Rev.* B **28** 5702
[7] Beck D E 1984 *Phys. Rev.* B **30** 6935
[8] Ekardt W 1984 *Phys. Rev. Lett.* **52** 1925; 1985 *Phys. Rev.* B **31** 6360; 1985 *Solid State Commun.* **54** 83
[9] Bertsch G and Ekardt W 1985 *Phys. Rev.* B **32** 7659
[10] Puska M J, Nieminen R M and Manninen M 1985 *Phys. Rev.* B **31** 3486
[11] Manninen M 1986 *Phys. Rev.* B **34** 6886
[12] Sheng P, Chou M Y and Cohen M L 1986 *Phys. Rev.* B **34** 732
[13] Stampfli P and Benneman K H 1987 *Physics and Chemistry of Small Clusters* ed. P Jena, B K Rao and S N Khanna (New York: Plenum)
Stampfli P and Benneman K H 1989 *Phys. Rev.* A **39** 1007
[14] Brack M 1989 *Phys. Rev.* B **39** 3533
[15] Kresin V 1988 *Phys. Lett.* **133A** 89; 1989 *Phys. Rev.* B **39** 3042
[16] Knight W D, Clemenger K, de Heer W A and Saunders W A 1985 *Phys. Rev.* B **31** 2539
[17] Hohenberg P and Kohn W 1964 *Phys. Rev.* **136** 864
[18] Kohn W and Sham L J 1965 *Phys. Rev.* **140** 1133
[19] Stott M J and Zaremba E 1980 *Phys. Rev.* A **21** 12
[20] Zangwill A and Soven P 1980 *Phys. Rev.* A **21** 1561
[21] Serra Ll, Garcias F, Barranco M, Navarro J, Balbás C and Mañanes A 1989 *Phys. Rev.* B **39** 8247
[22] Bohigas O, Lane A M and Martorell J 1979 *Phys. Rep.* **51** 267
[23] Lipparini E and Stringari S 1989 *Phys. Rep.* **175** 103
[24] Marshalek R and da Providencia J 1973 *Phys. Rev.* C **7** 2281
[25] Pines D and Noziéres P 1975 *The Theory of Quantum Liquids* (New York: Benjamin)
[26] Ekardt W 1985 *Phys. Rev.* B **32** 1961
[27] Kirzhnits D 1967 *Field Theoretical Methods in Many Body Systems* (Oxford: Pergamon)
[28] Bohr A and Mottelson B R 1975 *Nuclear Structure* vol II (New York: Benjamin)
[29] Lang N D and Kohn W 1973 *Phys. Rev.* B **7** 3541
[30] Sorbello R S 1983 *Solid State Commun.* **48** 989
[31] Parks J H and Stephen A M 1989 *Phys. Rev. Lett.* **62** 2301
[32] Charlé K P, Shulze W and Winter B 1989 *Z. Phys.* D **12** 471
[33] Rubio A and Balbás L C unpublished
[34] Perdew J P and Zunger A 1981 *Phys. Rev.* B **23** 5048
[35] Ekardt W and Penzar Z 1986 *Solid State Commun.* **57** 661
[36] de Heer W A, Selby K, Kresin V, Masui J, Volmer A, Chatelein A and Knight W D 1987 *Phys. Rev. Lett.* **59** 1805
[37] Selby K, Vollmer M, Masui J, Kresin V, Kruger M, de Heer W A and Knight W D 1989 *Z. Phys.* D **12** 477